Patched roughness in highly turbulent Taylor-Couette flow

TAI Ngan Cheung
The Chinese University of Hong Kong
Supervised by Dennis Bakhuis
Physics of Fluid, University of Twente

September 30, 2018

Abstract

The effect of periodic roughness pattern on highly turbulent Taylor-Couette flow in the Twente Turbulent Taylor-Couette (T^3C) apparatus is investigated. It is shown that the roughness can significantly increase the torque on the inner cylinder, and the Nusselt number Nu_ω scales as $Ta^{0.45\pm0.01}$ in the ultimate regime. If the thinner stripes of roughness were applied, the torque becomes larger since the turbulence intensity is higher in those cases, which can be reflected from the fact that the variance of angular velocity shows periodic strong peaks at the location of roughness. Moreover, the roughness also influence the row structure in Taylor-Couette flow. Not all the results are included in this report since the research is still ongoing and results obtained so far is not yet complete.

1 Introduction

Turbulence is a daily life phenomenon. For example, the motion of smoke, the rapid flow of the water in a river, etc. Turbulent flow is characterized by high Reynolds Number Re which is defined as $Re = \frac{uL}{\nu}$, where u is the characteristic velocity of the fluid, L is the characteristic length of the geometry, ν is the kinematic viscosity. Flows are said to be turbulent if $Re > 4000$ in general. In the study of turbulence, the historical Taylor-Couette flow has been widely studied. However, the study of the effect of roughness on the system is scarce.[1] In this study, the effect of the pattern of the roughness on highly turbulent Taylor-Couette flow is investigated. Different configurations of roughness patterns were applied onto the surface of the inner cylinder (Fig.1), while the outer cylinder remained smooth. For all the configurations, periodicity holds and the roughness coverage for the middle cylinder was kept constant at 56%. The $\frac{s}{d}$ value ranged from 0.31 to 3.78, where s is the width of each individual roughness strip and d is the gap width between the outer and inner cylinders. The parameters of the T^3C apparatus is listed in Table 1. The inner cylinder is decoupled into

three parts: top, middle and bottom ones. Each part has its own temperature sensor. They can also have their own torque sensor. In this research project, Taylor-ramp and a-ramp were carried out, and torque measurement is done only for the middle part. The dependence of the non-dimensional torque - the Nusselt number Nu_ω on the Taylor number Ta and the ratio of the angular velocity a of the inner and outer cylinder was studied. In the mean time, with the help of laser Doppler anemometry (LDA), and particle image velocimetry (PIV), the velocity profiles were provided. However, only some results of LDA and PIV were included in this report.

Parameter	value (m)
Radius of inner cylinder (r_i)	0.200
Radius of outer cylinder (r_o)	0.279
Height of middle cylinder (L_{mid})	0.536
Total height of the cylinder (L)	0.927

Table 1: Parameters of T^3C apparatus

2 Theory

For Taylor-Couette system, Reynolds numbers for the inner and outer cylinders are defined as $Re_i = r_i\omega_i d/\nu$ and $Re_o = r_o\omega_o d/\nu$, respectively.Taylor number is given by

$$Ta = \frac{1}{4}\sigma d^2(r_i + r_o)^2(\omega_i - \omega_o)^2\nu^{-2}$$

where $\omega_{i,o}$ is the angular velocity of the inner and outer cylinders respectively, and sigma can be interpreted as "geometrical" Prandtl number according to the theory by Eckhardt, Grossmann and Lohse (EGL theory).[2] It is calculated as $\sigma = [(1+\eta)/2\sqrt{\eta}]^4$, where η is the ratio r_i/r_o. $\eta = 0.716$ for this setup.
Suggested by EGL theory, torque τ can be non-dimensionalized in the following way and is called "Nusselt number",

$$Nu_\omega = \frac{\tau}{2\pi L_{mid}\rho J^\omega_{lam}}$$

where ρ is the density of the fluid, J^ω_{lam} is the angular velocity flux in the laminar case. J^ω_{lam} can be calculated analytically from the Navier-Stoke's Equation and the result is shown below

$$J^\omega_{lam} = 2\nu r_i^2 r_o^2 \frac{\omega_i - \omega_o}{r_o^2 - r_i^2}$$

In this study, the data from the T^3C apparatus is analyzed with the common power-law ansatz for the dimensionless torque $Nu_\omega(Ta, a) = f(a)Ta^\gamma$. By definition,

$$a = -\frac{\omega_o}{\omega_i}$$

Here, ω_i is defined as always positive while ω_o is defined to be positive for co-rotation and negative for counter rotation. In analogy to Rayleigh-Benard convection, it is postulated that an ultimate regime exists for TC flow.[1] In the study of Zhu *et al.*, they showed that the ultimate regime exist experimentally for high Ta number, and determined the scaling factor γ in several cases. In this study, Ta number goes up to $\sim O(12)$, and the scaling factor found in this study is in great agreement with that found by Zhu *et al.*.

3 Methods

In the experiment, water is used and sandpaper strips with sharp grain points were sticked on the innner cylinder as roughness. A scan of the surface is shown in Fig. 2. Throughout the experiment, temperature of the fluid was kept approximately constant at 21 ± 0.5^oC. So that viscosity μ of the water can be approximated using the following formula.

$$\mu = (2.414 \times 10^{-8}) \times 10^{247.8/(T-140)}$$

where T is the temperature of the water in Kelvin, and is direcly measured by the temperature sensor installed inside the inner cylinder. The error of this approximation is about 2.5%. At the mean time, the density of the water (in kg/m^3)was determined using the following formula

$$\rho = 1000(1 - \frac{T + 288.9414}{508929.2(T + 68.12963)}\sqrt{T - 3.9863})$$

On the other hand, techniques of LDA and PIV were applied for obtaining the information of the velociy field. In the following, a brief introduction of these two techniques is included.

3.1 Laser Doppler anemometry (LDA)

LDA was adopted for local velocity field measurement. The schematic diagram was shown in Fig.3. A laser beam is splited into two and one of them has a slight shift in frequency. At the position where the beams overlap, interference pattern occurs. Seeding particle which is assumed to flow with the fluid loyally without afftecting the flow is added to the system. The particles absorb the light and re-emit light. The re-emitted light enters the photon-detector and gives a series of signal while the particles are passing through the overlapping region. The intensity of the signal is proportional to the intensity of the re-emited light, which is also proportional to the intensity of the absorbed light. Since the the particles are passing through a region of intereference pattern, the signal due to the re-emitted light has also the same pattern. The separation of the peaks can be determined with high accuracy so one of the components of the velocity vector can be determined as well. In this project, the angular and vertical velocity components at different points along the vertical line at

$r = \frac{r_i + r_o}{2}$ were measured using this method. 50 points on the lower-half of the system were selected for the measurement. Since two components of the velocity vector were measured, four laser beams (splited from two laser beams) were required in the experiment.

3.2 Particle Image Velocimetry (PIV)

PIV was used for obtaining a 2-D plane of velocity field. Similarly to the principle of LDA, a pulses of thin laser sheet is shined onto the region to be measured. The particles within the region absorb light and re-emit it in all direction. The re-emitted light was captured by a camera. The bright dots in the photo indicate the position of the paticles at that moment. After a short time Δt, another pulse of laser sheet is shined onto the region and another photo is captured. Then, the position of the particles at two instance is obtained. The average 2-D velocity within Δt of each particle can be measured. In this experiment, velocity field on the $r - \theta$ plane were measured using this method. For each configuration in Fig.1, such velocity field measurement was repeated for three different position: the miiddle of the roughness, the middle of the smoothness, the border between roughness and smoothness.

4 Measurement

In this project, Ta-ramp, a-ramp were done. For the Ta-ramp experiment, the inner cylinder rotated from 0 Hz up to $\sim$ 18 Hz, and Ta ranged from 0 up to $O(12)$. For a-ramp, ω_i increased from 9.1428π to 16π, while ω_o increased from -6.8572π to 0, and thus a ranged from 0 to 0.75. On the other hand, Ta-ramp measurement was repeated, for every configurations, for $\alpha = 1\%, 2\%, 3\%$ where α is the volume fraction of air. For $\alpha \neq 0$ cases, the inner cylinder rotated from 5 Hz up to $\sim$ 18 Hz.
PIV and LDA measurements were done for each configuration and with constant rotation frequency of 8Hz. Throughout all the experiments, temperature was approximately kept at constant of approximately 21 ± 0.5^oC.

5 Results and Discussion

In Fig.4a, the plot of Nu_ω versus Ta for full range is shown while the log-log plot of Nu_ω versus Ta is shown in Fig. 4b for high Ta only. As expected, ultimate regime exists for high Ta, and the scaling factor is approximately 0.45 ± 0.01 which is in great agreement with the result in [2]. It can be also clearly seen that in Fig. 4a, the torque required for keeping the inner cylinder rotating is larger for thinner roughness stripes, except for the case of the thickest strip. The reason why configuration 1 does not follow the trend can be due to the difference of the boundary conditions to other configurations. Since only the torque for the middle cylinder were measured, and there was no roughness stripes on the top, bottom cylinders only for the first configuration, thus the boundary condition

for the middle cylinder could be difference. Meaning that the flow produced by configuration 1 might not be a part of that produced by a infinitely long Taylor-Couette appartus with periodic roughness pattern attached on it. It was originally attempted to generate a section of the flow generated by an inifinitely long TC apparatus with periodic roughness along the middle cylinder, using those configurations. It might be probably failed for the first configuration. For comparison, the data for no roughness is also presented on the plots. The torque increases enormously by a factor of ~ 1.5 comparing to the situation of no roughness.

The trend of increasing torque with decreasing $\frac{s}{d}$ value can be explained by the result of LDA shown in Fig. 5. In Fig. 5a., mean of the angular velocity is plotted against height z while dependence of the variance of the angular velocity on z is presented on Fig. 5b. Suprinsingly, the mean of the velocity shows no periodicity. Nevertheless, the variance indeed has obvious period which is the same as that of the roughness stripes. At the position where the roughness stripes located at, there is high variance on the angular velocity. This imply that where the roughness strips are, the turbulence instensity is higher. For smaller roughness stripes, more peaks present, and thus leads to stronger torque on the inner cylinder.In Fig. 6, the radial component of the average velocity field is plotted on the $r - z$ plane. Interestingly, flow next to the roughness stripes tends to move out from the inner cylinder while the flow next to the smooth surface tends to move inwards. The roughness seems to influence the row structure of the Taylor-Couette flow.

References

[1] Xiaojue Zhu and Verschoof, Ruben Adriaan and Dennis Bakhuis and Huisman, Sander Gerard and Roberto Verzicco and Chao Sun and Detlef Lohse *Wall roughness induces asymptotic ultimate turbulence*. Nature physics. 14(1745-2473), 417-423, 2018

[2] Dennis P. M. van Gils, Sander G. Huisman, Siegfried Grossmann, Chao Sun, Detlef Lohse *Optimal Taylor-Couette turbulence*. J. Fluid Mech. 706, 118, 2012

6 Figures

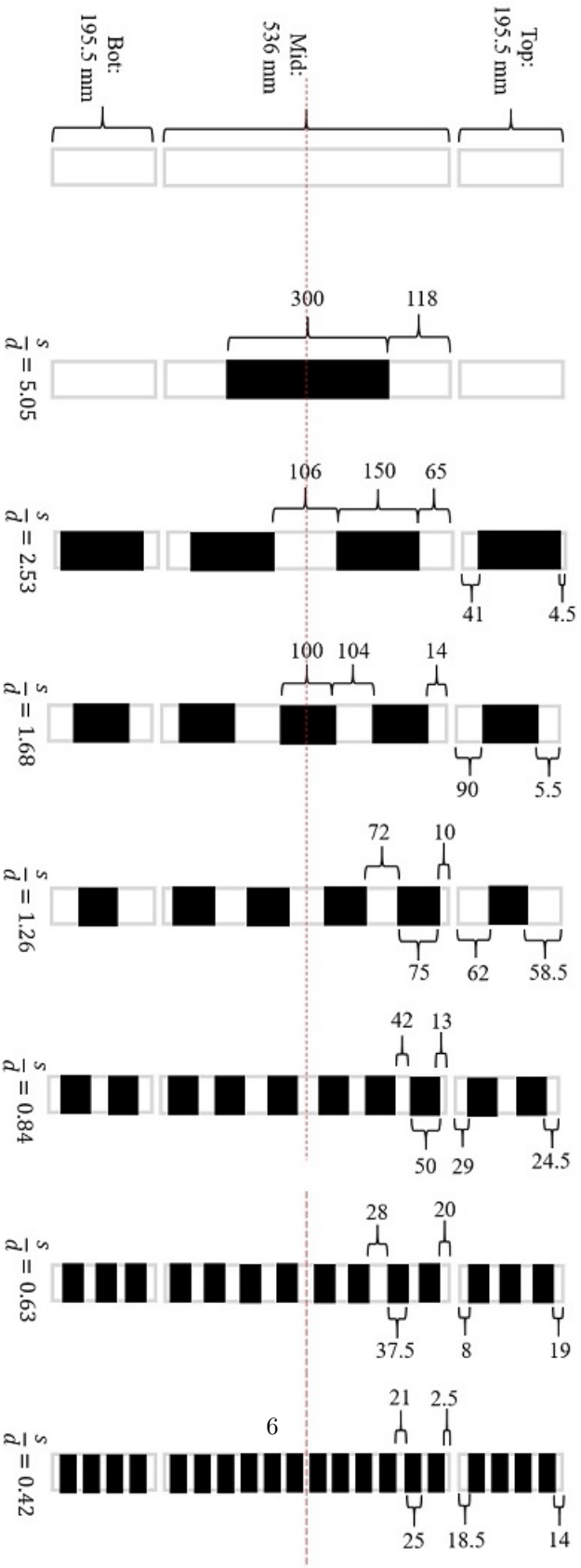

Figure 1: Configuration of all the experimental setup

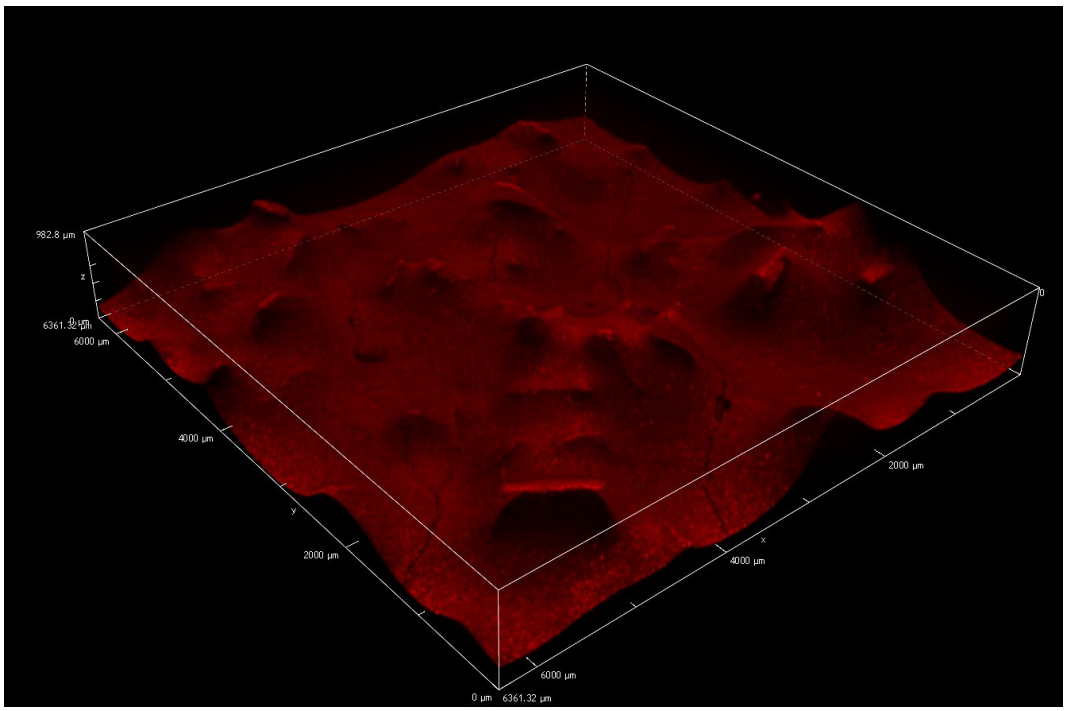

Figure 2: A surface scan of the roughness surface

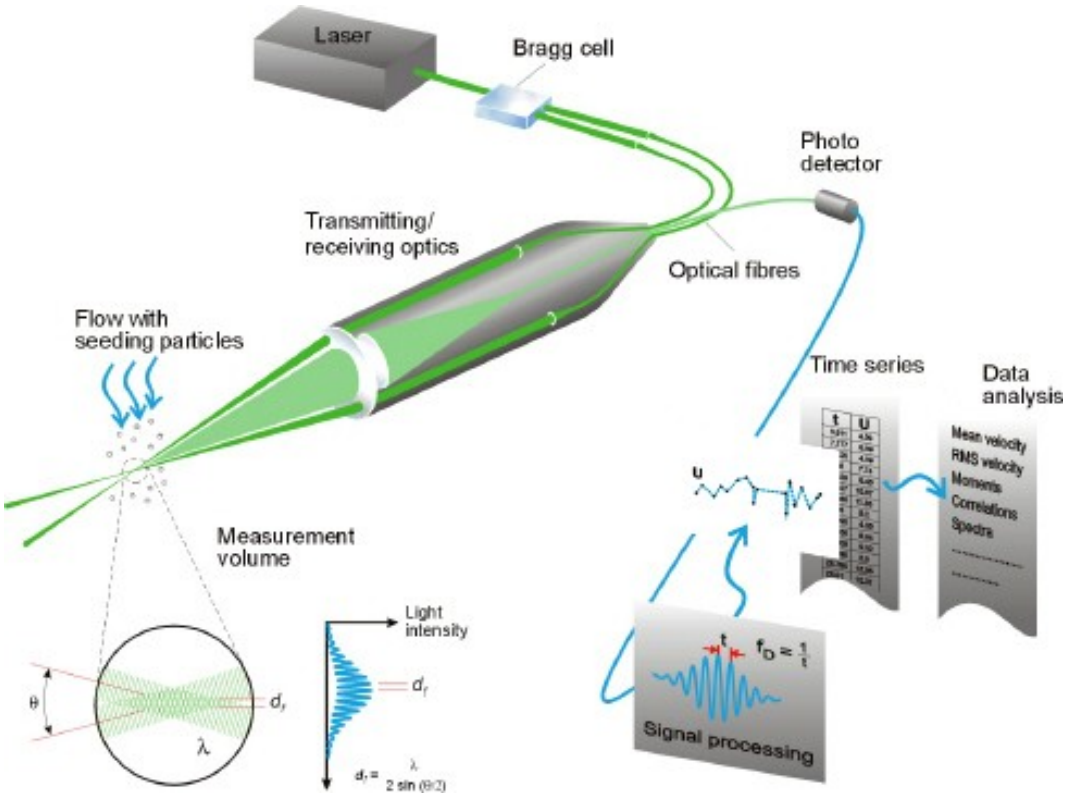

Figure 3: A schematic diagram for LDA

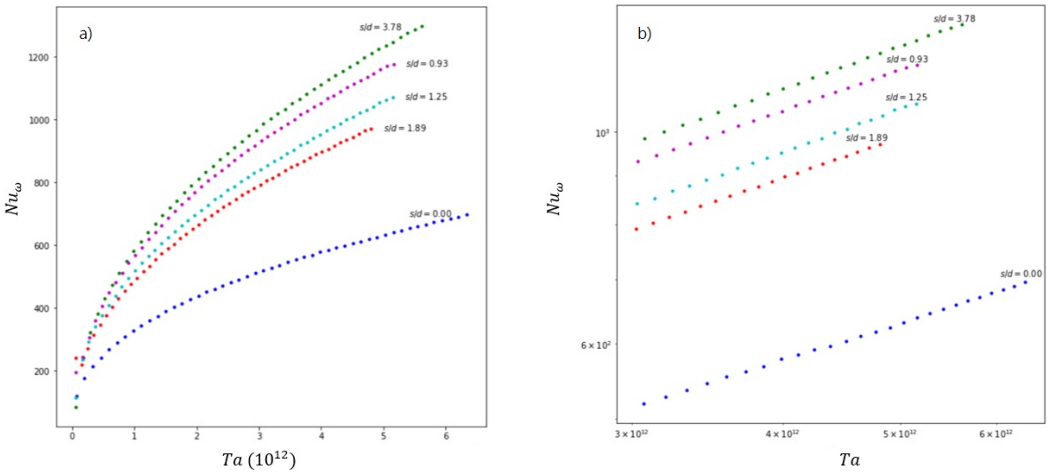

Figure 4: a) The plot of Nu_ω versus Ta. b) The log-log plot of Nu_ω versus Ta for high Ta

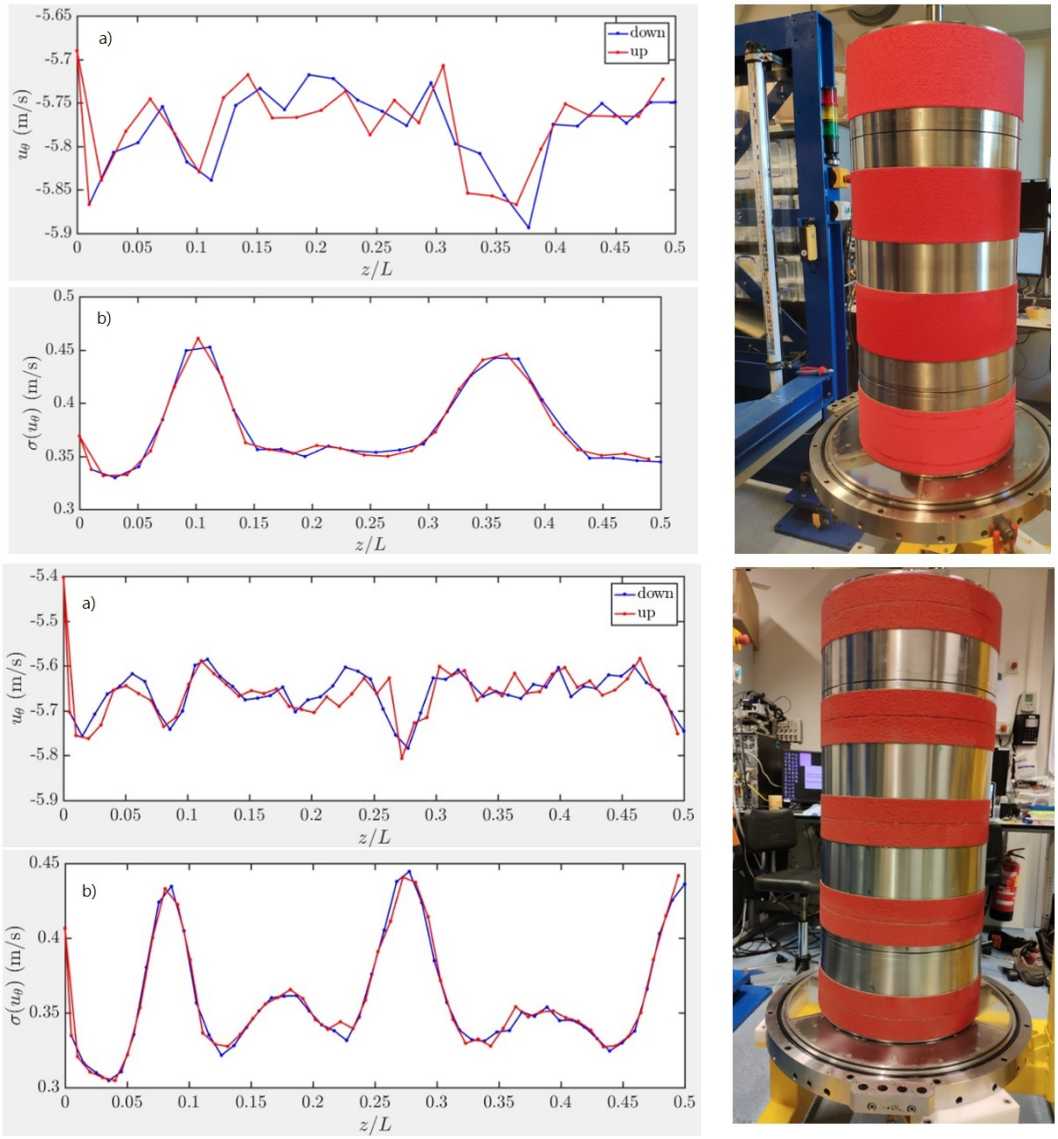

Figure 5: a) The mean of the angular velocity is plotted against height. b) The variance of the angular velocity is plotted against height. The error of the measurement is less than 1% on average.

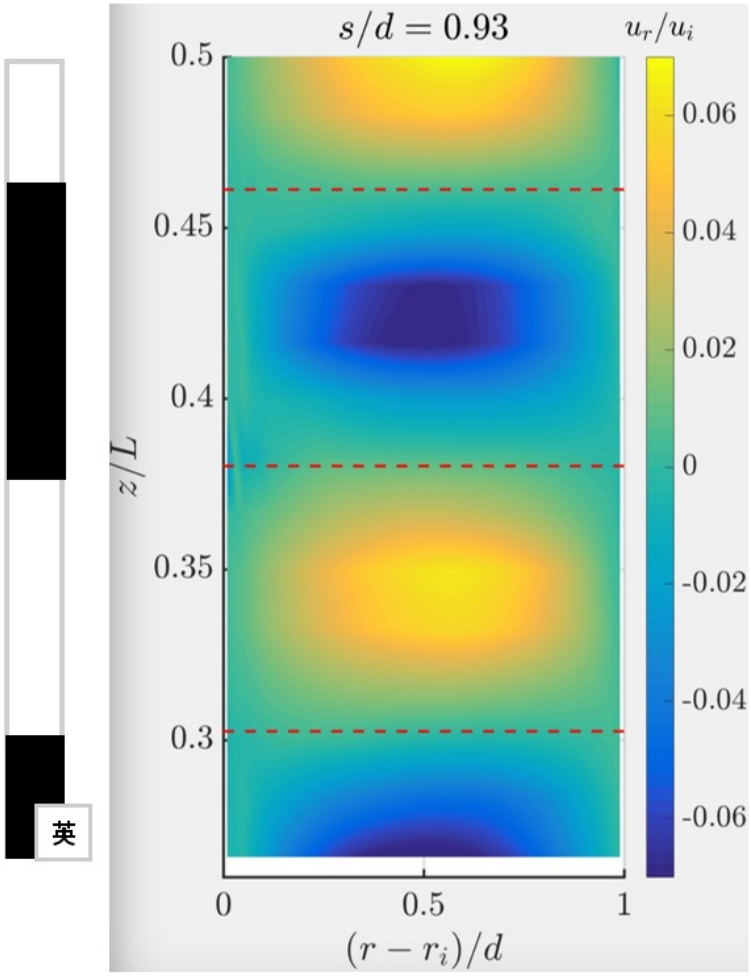

Figure 6: The radial component of the velocity field is plotted on the r-z plane.